NUMERICAL SIMULATION OF FLOW PATTERN AT A DIVERGENT PIER IN A BEND WITH DIFFERENT RELATIVE CURVATURE RADII USING ANSYS FLUENT

Kooshyar Lahsaei[1], Mohammad Vaghefi[1], Chonoor Abdi Chooplou[2*], Farid Sedighi[1]

[1] Civil Engineering Department, Persian Gulf University, Bushehr, Iran
[2] Faculty of Civil and Environmental Engineering, Tarbiat Modares University, Tehran, Iran.

ARTICLE INFO

***Article history*:**
Received: 19.10.2021.
Received in revised form: 12.04.2022.
Accepted: 19.04.2022.

Keywords:
Inclined Piers
Flow Pattern
180-Degree Bend
Relative Curvature Radius
ANSYS FLUENT Numerical Model

DOI: https://doi.org/10.30765/er.1894

Abstract:

In this work, the three-dimensional flow around piers in river meanders under rigid bed conditions was modeled. The software ANSYS FLUENT was used to perform the simulation. The study was carried out in a 180° curve accompanied by cylindrical piers with a diameter of 5 cm and a slope angle of 21° under rigid bed conditions. The results of the comparisons showed that this model can help simulate the flow pattern around inclined bridge piers in bended channels with acceptable accuracy. To analyze the flow pattern, the work was followed by studying the effect of the parameters that affect the physics of the problem: the relative radius of curvature of the curve, the location of the piers within the 180° curve, and the arrangement of the piers relative to the flow direction. The results showed that increasing the relative radius of curvature as well as the range of the bend reduced the tangential velocity values; the minimum tangential velocity value occurred at a relative radius of curvature of 5. With the pier group installed in the direction of flow, the maximum secondary flow power occurred at the 60° position at about 18.8%, while with the pier group installed across the flow, the maximum secondary flow power occurred at the 120° position at 14.2%. A comparison of the vorticity at the perpendicular and downstream positions showed that the vorticity values at the 60° and 120° positions were greater than the corresponding values at the 90° position in both cases.

1 Introduction

The meander pattern is the governing pattern in rivers as natural systems. The flow pattern in a meander is more complicated than in a straight river. The centrifugal force acting on the flow as it enters the bend is the major force acting on flows in bends. This force causes a change in the lateral slope of the water surface in the bend. The difference in depth between the outer and inner bends creates a lateral pressure gradient within the bend. When this pressure gradient overcomes the centrifugal force, a type of flow called secondary flow develops in the lateral direction within the bend. When the lateral secondary flows combine with the main flow along the path, a helical flow develops in the curve. This helical flow plays the main role in changing the shear stress distribution across the channel bed and in the formation and development of bed variations.

One of the most important factors involved in bridge destructions is the scour around the pier.

Therefore, it is important to understand the mechanism to prevent or reduce the impact.

River bed materials are erodible, but the extent of such erosion depends on time; therefore, river beds covered with granite take years to erode, while sand beds undergo the maximum scour depth over a highly short period of time. In addition to river and bed structures as some of the key factors of erosion, hydraulic causes also play a significant role in incidence of such a phenomenon. Among such causes, the pattern of the

* Corresponding author
E-mail address: a.chonoor@modares.ac.ir

flow passing through the piers is worth mentioning. The presence of bridge piers inside the bend affects the helical flow pattern, further complicating the flow behavior. Moreover, installation of bridge piers on the flow path entails changes in the flow structures and generation of vortices around the pier. These vortices are demonstrated as the main causes of scour around bridge piers. Horseshoe vortices present at the fore-end and wake vortices appearing in back of the pier represent the key characteristics which play a role in generating scour about bridge piers.

Considering the explanations on flow patterns in curves and at bridge piers, the flow pattern in the curve as well as the flow impediment at the pier contributes to the complexity of flow pattern conditions around the pier in the curve. Since some bridges are built on river channels in the curve, understanding the flow pattern around these types of piers can help identify the scour pattern. Therefore, further study of flow patterns around bridge piers in meanders is considered essential.

A number of researchers have always made efforts to examine the flow structure around bridge piers with experimental and numerical methods. Among the research conducted around this topic, the following may be stated: Mendoza-Cabrales (1993) employed the standard K-ϵ turbulence model in order to solve the 3D velocity in the vicinity of transverce cylindrical piers [1]. Rodi (1997) compared the flow around a square pier by using RANS and LES models. They reckoned that the results obtained from calculations of LES were more efficient than those of RANS [2]. Richardson and Panchang (1998) utilized FLOW-3D in order to simulate the flow around a cylindrical pier in a straight path and to investigate the effect of local scour on flow pattern [3]. Yen et al. (2001) integrated the 3D model of the flow with the scour model, and were able to simulate variations in bed and flow pattern around the bridge pier. In their study, LES model was incorporated for modeling turbulence and shear stress [4]. Graf and Istiarto (2002) used ADVP velocimeter to examine the flow pattern around a cylindrical bridge pier in a straight path with mobile bed, and then reported the vortices occurring around the pier [5]. Ali and Karim (2002) employed FLUENT to simulate the flow around a cylindrical pier located in a straight path three-dimensionally, and then used the results to propose a semi-empirical and semi-numerical relation for the maximum scour depth in front of the pier [6]. Salaheldin et al. (2004) utilized FLUENT for simulation of the flow separating around the bridge pier under clear water conditions. Calculations were made by using different turbulence models. There was little difference found between the bed shear stress results obtained from the k-ε turbulence model and those from the experimental results [7]. Ettema et al. (2006) incorporated their own experimental data in order to demonstrate a direct relationship between balanced scour depth and turbulence intensity. Three important factors – the pier diameter, the bed particle diameter, and the flow depth – influenced the balanced scour depth around the pier; the size of the vortices behind the cylindrical pier of a smaller diameter was approximately twice the size of those behind the pier of a larger diameter [8]. In an experimental study, Beheshti and Ashtiani (2009) investigated a three-dimensional turbulent flow field around a bridge pier installed in a straight path with a steady bed [9]. Das et al. (2013) conducted a study on the flow pattern in a laboratory channel with a straight reach by employing ADV velocimeter. The pier employed in their experiment was paired and located on the plane in a streamwise direction. They first calculated the flow hydraulic parameters, and then illustrated the created horseshoe vortices by drawing the streamlines [10]. Vaghefi et al (2015) conducted a numerical study of the effect of a support structure on the flow pattern around a T-shape spur dike in 90◦ bend channel. The test results showed that by increasing the support structure distance from 3L up to 9L, the power of secondary flow around the T-shape spur dike decreased by 40–120% and the length of the separation zone increased from 0.8 to 2.5 times bigger than the length of the T-shape spur dike [11]. Ehteram and Meymand (2015) carried out flow and sediment simulations at a bridge constriction by incorporating SSIIM2 software in three directions in a straight reach. They used this model on a mobile and rigid bed, and then compared the results with experimental data. This comparison developed a 3D model for appropriate simulation of velocity and water surface [12]. Hamidi and Siadatmousavi (2017) incorporated SSIIM numerical model in order to conduct a numerical simulation of the flow pattern and scour around bridge piers in a straight path. As demonstrated in their results, although SSIIM numerical model was able to successfully estimate the scour depth in front of the piers adjacent to each other, it overstated the depth of scour at the gap between the piers [13]. Asadollahi et al. (2020) utilized SSIIM mathematical model in examining the three-dimensional flow and scour pattern around sets of piers arranged in a transverse direction. Their findings suggested that altering the bridge piers' position in the channel had an insignificant effect on the value of the maximum scour, while the value of the maximum sedimentation rose by 12% when the piers were displaced from 60 degrees to 90 degrees; however, moving them from 90 to 120° entailed a 42% decrease in the maximum sedimentation [14]. Researchers including Vaghefi et al. (2016),

Wang et al. (2016), Khaple et al. (2017), Vaghefi et al. (2018), Abdi Chooplou and Vaghefi (2019), Safaripour et al. (2020), Vaghefi et al. (2020), Moghanloo et al. (2020), Sedighi et al. (2020), Dehghan et al. (2021), Keshavarz et al. (2021) and Solati et al. (2021) examined the scour and flow pattern around bridge piers in a laboratory [15-26]. Mulahasan et al. (2021) developed a numerical model of the flow around a vertical emergent sidewall abutment in an open channel flow, eventually showing a good match between experimental and numerical results of the water surface profiles. They showed that increasing discharge increased the maximum pressure in front of the constriction [27]. Vaghefi et al, (2021) explored the scour around a triad series of vertical piers in a bend. By considering the most critical parameters, such as the relative radius and the bridge pier position, they demonstrated that their model was able to not only approximate but also foresee the maximum scour and sedimentation [28]. Indulekha et al. (2021) modeled the flow pattern around groynes in meandering paths by developing a 3D numerical model with varied inclinations of groynes. The results referred to the efficiency of the model to study flow and turbulence regarding groynes in meanders [29]. Das et al. (2022) studied boundary shear stress in non-prismatic compound channel considering the relative flow depth and divergence angle. They were able to validate their simulations using four turbulence models of LES, k-ε, k-ω, and SST [30]. Chakravarthy et al. (2022) utilized ANSYS to model flows running into an off-taking channel while considering the flow rate. They used two varying turbulence models, which proved acceptable agreement with the analytical estimations [31]. Tripathi and Pandey (2022) examined the flow characteristics at a T-shaped spur dike in a reverse-meandering channel with a rigid bed using RNG turbulence model, focusing on the Froude number, velocity distribution, etc. They eventually compared the results with those of a channel empty of any structures [32].

Given the fact that changing the curvature radius parameter under laboratory conditions is extremely difficult and expensive, this study examined the effect of the relative curvature radius of the bend (R/B), and the effect of the position of the piers in the 180° bend, the effect of the arrangement of the piers with respect to the flow direction on the flow pattern around a divergent twin pier group and the effect of the piers' positioning by using ANSYS FLUENT numerical model. The results obtained through measurements of flow velocity by ADV velocimeter around the above laboratory model in the 180° bend were used in order to validate the results obtained via numerical modeling.

2 Introduction of Equations Governing the Flow Field

ANSYS is an engineering software program selected from analytical tools which use the Finite Volume Method (FVM) for simulation and analysis. In the finite volume method, the solution range is broken down to a finite series of control volumes; then general conservation (continuity) equations of mass and momentum are solved in this set of control volumes. The general form of continuity and momentum equations is used in the software as follows [33]:

$$\frac{\partial \rho}{\partial t}+\frac{\partial}{\partial x_i}(\rho u_i)=0 \tag{1}$$

$$\frac{\partial}{\partial t}(\rho u_i)+\frac{\partial}{\partial x_j}(\rho u_i u_j)=-\frac{\partial p}{\partial x_i}+\frac{\partial \tau_{ij}}{\partial x_j} \tag{2}$$

In the above equations: t is time, ρ is fluid density, P denotes pressure, τij represents shear stress tensor, and u is velocity. By discretizing the flow equations in the volume of the controls, the partial differential equations are separated into a set of algebraic equations, and then all algebraic equations are solved numerically to obtain the solution field.

In this research, the Standard k-e model is used for simulation. To solve the perturbation equations of this model in ANSYS FLUENT software, the solutions of equations (3) and (4) are used to calculate the amounts of Turbulent Kinetic Energy and Turbulent dissipation rate in each iteration, respectively [33]:

$$\frac{\partial}{\partial t}(\rho k)+\frac{\partial}{\partial x_i}(\rho k u_i)=\frac{\partial}{\partial x_j}\left[\left(\mu+\frac{\mu_t}{\partial_k}\right)\frac{\partial k}{\partial x_i}\right]+G_k+G_b-\rho\varepsilon-Y_m+S_k \tag{3}$$

$$\frac{\partial}{\partial t}(\rho \varepsilon)+\frac{\partial}{\partial x_i}(\rho \varepsilon u_i)=\frac{\partial}{\partial x_j}\left[\left(\mu+\frac{\mu_t}{\partial_\varepsilon}\right)\frac{\partial \varepsilon}{\partial x_i}\right]+G_{1\varepsilon}\frac{\varepsilon}{k}(G_k+G_{3\varepsilon}G_b)-G_{2\varepsilon}\rho\frac{\varepsilon^2}{k}+S_\varepsilon \tag{4}$$

In the above equations, μ_t is turbulence viscosity, G_k represents turbulent kinetic energy production rate based on the average flow velocity gradient, G_b is turbulence kinetic energy production rate based on the buoyancy force, Y_m denotes the share of the effects of compressed turbulence fluctuations up to the limit of the total decay rate, and S is the average tensor rate modulus of strain. Equations' constants as well as Prandtl numbers are defined as below [33]:

$$G_{1\varepsilon}=1.44 \qquad G_{2\varepsilon}=1.92 \qquad \partial k=1.0 \qquad \partial\varepsilon=1.3$$

3 Validation of the Numerical Model

The validation process was followed using ANSYS software by applying the experimental data from the channel with R/B=2, where R denotes the bend's central radius of curvature and B represents the channel width. The channel under investigation is located in the advanced laboratory of hydraulic structures in the Faculty of Engineering in Persian Gulf University. It is set up with a straight 6.5-m-long path at the upstream side and a straight 5.1-m-long path at the downstream side. A 180° bend with an internal radius of 1.5 m and an external radius of 2.5 m functions as the connection between the two paths. The channel is 90 cm at height and 100 cm at width. The approach flow rate in this channel is 70 liters per second, and the flow 18 cm high at the bend entrance under incipient motion conditions. The flow pattern experiments of the V-shaped pier group with a diameter of 5 cm were conducted under rigid bed conditions with installations on the plane transverce to the flow direction and an inclination angle of 21° at the 90° position from the bend entrance. Validation was made possible by using ANSYS software to model a channel similar to the laboratory channel, and 3D flow velocities were also compared. Results referred to the capability of ANSYS numerical model to simulate the flow in 180° bent channels with rigid beds. A view of the channel, along with a schematic of V-shaped piers, is presented in Fig. 1.

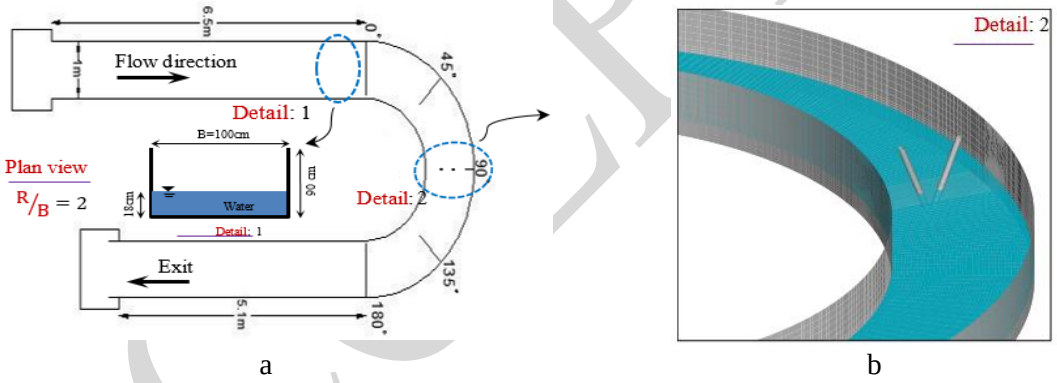

a b

Fig. 1. A) a view of the channel and b) a schematic of V-shaped piers.

One of the issues which must be addressed in every numerical research is mesh independency of the solution. The size of the selected mesh for numerical solutions always influences the results of the solution; therefore, an optimum mesh must be considered for the solution. It may be concluded from the number of errors obtained from the mesh between the experimental model and the numerical model that a 148640-mesh cuboid was employed in the hexahedron mesh. Table 1 provides the specifications of the meshing used in the numerical model, the root mean square error (RMSE) and the mean absolute error (MAE) values at the simulated free surface profile. As seen in Table 1, the difference between the results of meshing 2 and 3 is negligible, and meshing 2 is opted for computational field detachment. Fig. 2 illustrates a view of the mesh throughout the bend and the plan around the piers.

Table 1. Meshing specifications, RMSE and MAE of the simulated free surface profile.

Meshing	Number of cells	RMSE, (m/s)	MAE, (m/s)
1	8120	4.294	4.153
2	148,640	0.191	0.119

3	279,820	0.188	0.118
4	454,290	0.275	0.224
5	764,861	1.403	1.554

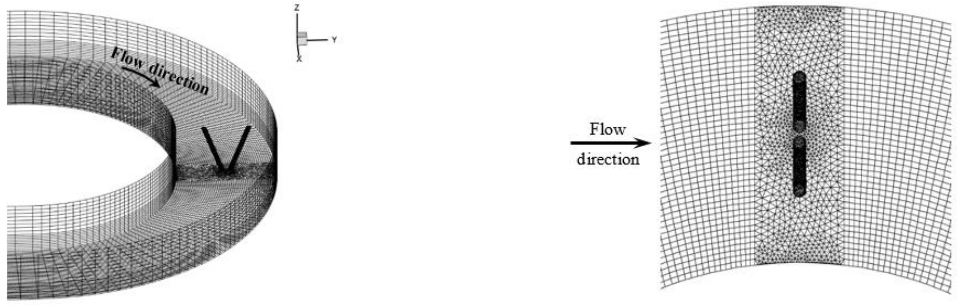

a b

Fig. 2. A view of the points' mesh in flow pattern collection a) throughout the bend, and b) in the plan around the piers.

Figs. 3 and 4 depict 3D flow velocity distributions for channel cross sections at the upstream and downstream sides of the V-shaped pier group in both the experimental and numerical models. In these figures, the horizontal axis represents the channel width (B) and the vertical axis is the side slope (Z) non-dimensionalized using the water depth (y) at the beginning of the bend. The secondary flow was generated at the cross section as the flow entered the bend; hence, the streamlines in proximity of the water surface were directed towards the outer bank, and those near the bed were directed towards the inner bank. The tangential velocity in Fig. 3 (a) in this section is positive in every region in both the numerical and experimental models; i.e. it was in the direction of the mainstream. As is evident from the tangential velocity profiles, the velocities were minimal in proximity of the bed, yet they increased from the bed to the water surface due to depreciation of the boundary layer. The radial velocity (Fig. 3(b)) at this section was positive in every region; i.e. it was directed towards the inner bank. From the level near the bed up to the level of 0.55 y, the radial velocity in the experimental model was larger than that in the numerical model, while the velocity profile from that level to the water surface became almost linear and vertical; therefore, the velocity difference at different layers of this region was eliminated. The vertical flows at water surface were all down flows. Vertical velocity values at this level underwent great variations, most of which occurred at the outer bank (Fig. 3(c)). A comparison of Figs. 3 (a) to (c) indicates that tangential velocities had better correspondence than radial and vertical velocities. An investigation of 3D velocity profiles referred to a better match of experimental and numerical profiles at the upstream side of the V-shaped pier.

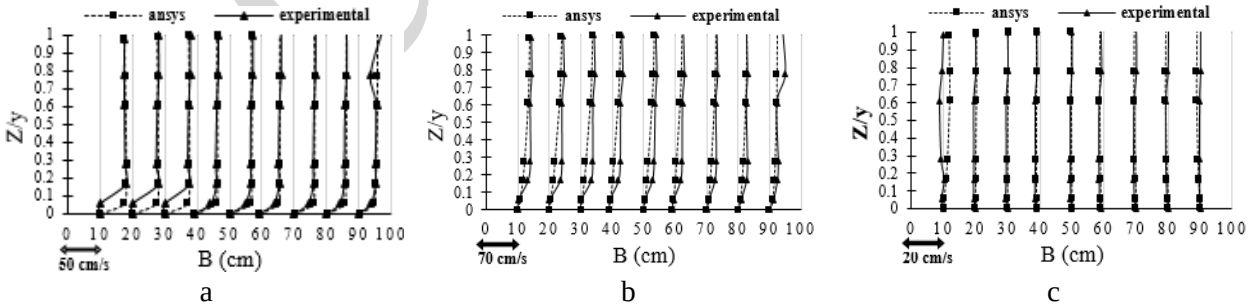

a b c

Fig. 3. Instances of a) tangential, b) radial, and c) vertical velocity profiles at the 60° cross section in the two numerical and experimental models.

Fig. 4(a) illustrates an identical and positive tangential velocity at the 120°section in both models. Due to the impact of the mainstream flowing downstream and the turbulence caused by presence of the pier, the radial velocity profile at upstream sections oriented towards the outer bank (Fig. 3(b)) and that at downstream sections oriented towards the inner bank (Fig. 4(b)). As depicted in Fig. 4(c), vertical velocity distributions did not enjoy an acceptable correspondence in the numerical and the experimental models at this section with

respect to either the direction or the magnitude of the velocities. This is mainly attributed to experimental data collection, employment of the side-looking probe for velocity data collection in proximity of the banks, and errors in data collection. The greatest difference between these two models was found in distribution of the vertical velocities at this section with respect to 10% range of the channel width away from the inner and outer banks. However, the velocities were similar at other cross sections of the channel.

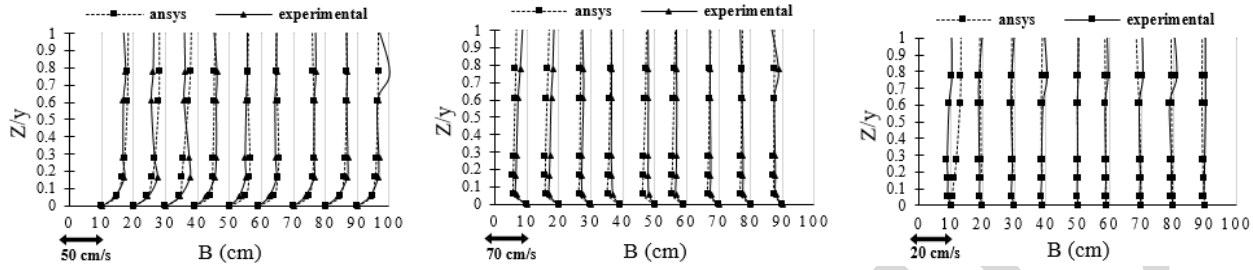

Fig. 4. Instances of a) tangential, b) radial, and c) vertical velocity profiles at 120°cross sections in the two numerical and experimental models.

Fig. 5 illustrates 3D flow velocities at the longitudinal section along mid-channel in proximity of the piers. Fig. 5(a) illustrates the tangential velocity distribution at the longitudinal section within 50% of the channel width away from the inner bank. Tangential velocity fluctuations are evident due to generation of return flows at the downstream sections of the pier,; a greater number of such fluctuations occurred in the numerical model. A study of the tangential velocities indicates that with the movement of the flow from the entrance to the end of the bend, the quantitative value of this parameter increased. The tangential velocity first increased from the bend entrance. Then it decreased in the second half of the bend at its outlet. This trend was observed in both the numerical and experimental models. As illustrated in Fig. 5(b), streamlines were redirected after impacting the pier, and in turn, led to creation of horizontal vortices at the downstream regions of the pier. Fig. 5(c) indicates that the vertical velocity profiles in both models and at the presented section match well. Correspondence of vertical velocities in the vicinity of the inner and outer banks in the numerical and experimental models decreased in comparison with that at mid-channel.

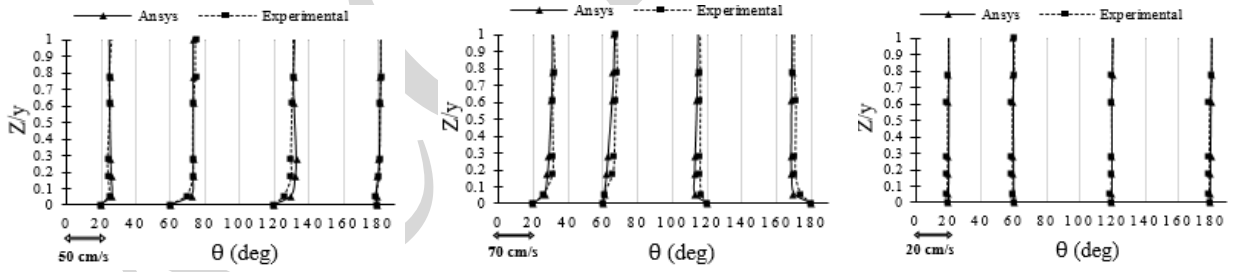

Fig. 5. Instances of a) tangential, b) radial, and c) vertical velocity profiles in the longitudinal profile at a distance of 50% from the inner bank in both numerical and experimental models.

Fig. 6 compares 3D velocity data in the numerical and experimental models. According to the bisector, velocity data were similar with an appropriate approximation, and most of them fell in the range of 20% error, which is itself a criterion indicating the similarity between tangential, radial and vertical 3D velocities in both the numerical and experimental models.

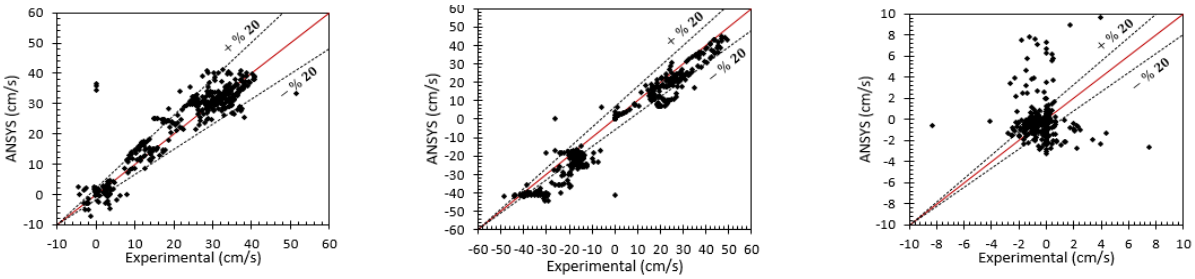

a b c

Fig. 6. A comparison between a) tangential, b) radial, and c) vertical velocity data in both numerical and experimental models.

The root mean square error and the mean absolute error in Table 2 helped the analysis of the error in ANSYS numerical model in comparison with experimental models. According to validations conducted in Table 2 and a comparison with resembling research [34], it may be concluded that ANSYS numerical model successfully simulated the flow pattern in the 180° bend hosting inclined piers.

Table 2. Error in ANSYS numerical model compared to the experimental model.

Row	velocity components	RMSE, (m/s)	MAE, (m/s)
1	U_θ	0.145	0.125
2	V_r	0.167	0.146
3	W_z	0.147	0.113

Table 3. Specifications of the models.

No	Abbr.	Position of the piers with respect to the flow direction	Position of the piers in the bend (degrees)	Relative curvature radius of the bend (R/B)
1	VT60R2	T	60	2
2	VT90R2	T	90	2
3	VT120R2	T	120	2
4	VT60R3	T	60	3
5	VT90R3	T	90	3
6	VT120R3	T	120	3
7	VT60R4	T	60	4
8	VT90R4	T	90	4
9	VT120R4	T	120	4
10	VT60R5	T	60	5
11	VT90R5	T	90	5
12	VT120R5	T	120	5
13	VS60R2	S	60	2
14	VS90R2	S	90	2
15	VS120R2	S	120	2
16	VS60R3	S	60	3
17	VS90R3	S	90	3
18	VS120R3	S	120	3
19	VS60R4	S	60	4
20	VS90R4	S	90	4
21	VS120R4	S	120	4
22	VS60R5	S	60	5
23	VS90R5	S	90	5

24	VS120R5	S	120	5

As follows, 24 different simulations were conducted based on Table 3 in order to study the effect of alterations in the relative curvature radius of the bend, the effect of relocation of the piers along the 180°bend, and the effect of the pier's positioning relative to the flow direction on the flow pattern around the divergent twin pier group. The second column of the table considers abbreviations for every simulation according to their features. V denotes the arrangement of the piers. T and S in model labels respectively represent installation of the piers in transverce and streamwise positions to the flow direction. As an instance, Model 1, here called VT60R2, simulates V-shaped piers set up in a transverce position to the flow at the 60° location in the bend with a relative curvature radius of 2.

4 Results and discussion

Figs. 7, 8, and 9 illustrate instances of cross sections at the site of the piers in either transverce or streamwise positions to the flow. The centrifugal force began to dominate the flow across the channel when the impact of the longitudinal pressure gradients subsided; then the secondary flow was observed as a single rotating cell at the cross section, which was known as the main or the primary secondary flow. It may be observed in Fig 7(a) and (b) that installation of V-shaped piers in a transverce direction to the flow with R=2B resulted in creation of three flow zones at channel width. The flow in the first zone, between the inner bank and the pier in its vicinity, was deviated towards the inner bank and the bed with an angle, and led to generation of a small vortex from the inner bank to a distance of 20% of the channel width up to a level of approximately 35% of the flow depth. In the second zone, between the piers, the flow was formed as down flow. The flow in the third zone, extending from the pier to the outer bank, attacked the outer bank and impacted the wall and the bed, and was then deviated towards the inner bank. It may be stated that flow deviation in this zone, as well as the vortex created in the first zone, is a suggestion of the secondary flow power. This flow still kept being generated despite the presence of piers. The trend mentioned above was found in the bend with R=4B. In the bend with R=4B, the main secondary flow inside the internal bend was observed as two vortices in two zones: the first zone appeared at 88% of the depth from the bed, and the second zone took place at 25% of the depth from the bed. Both vortices were generated in the range of 5% the depth from the inner bank. Given the cross section drawn at the site of the V-shaped piers on streamwise planes (Fig. 7-c and 7-d), the flow is under the influence of piers so that the impact of the lateral flow with the piers results in deviation of this flow towards the bed. Furthermore, with a larger curvature radius, as in Fig. 7 (d), the flow tends to create a counterclockwise vortex, i.e. the second secondary flow in the vicinity of the outer bank.

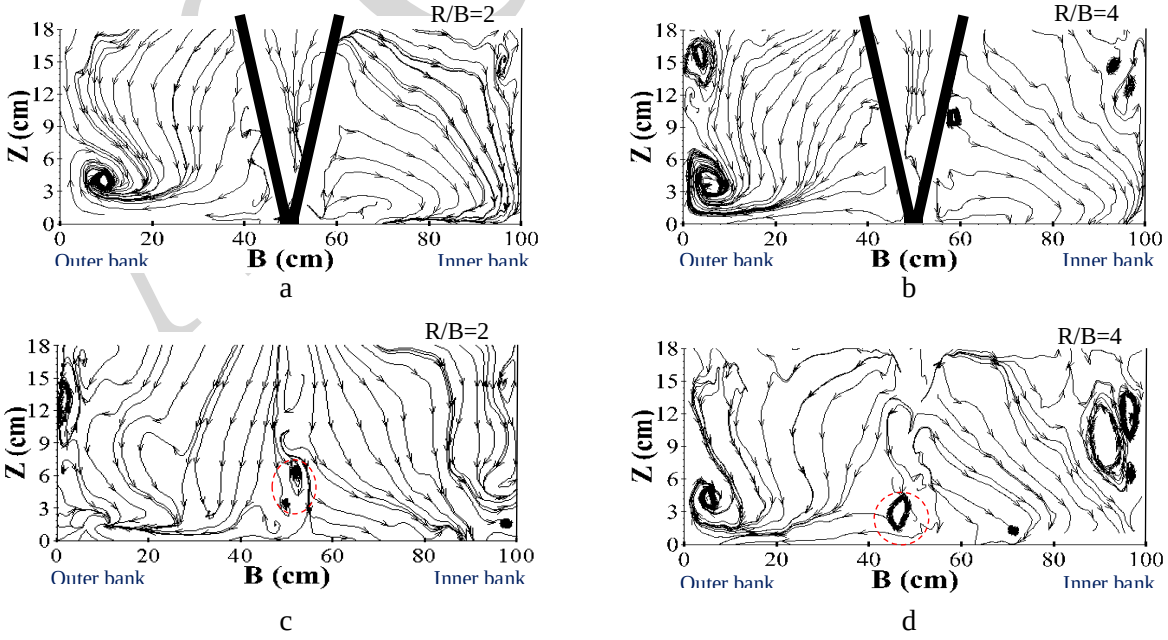

Fig. 7. An instance of the streamlines at the cross sections crossing the center of the pier groups, with the piers installed on a plane a) transverce and b) streamwise (c and d) to the flow direction at the 60° position with R=2, 4B.

This trend is illustrated at the 90° position in Fig. 8. According to Fig. 8 (a), the flow is deviated towards the bed, and scour is due to occur in this zone if the bed is not rigid. As seen in the figure, a large vortex occurred at the level of 22% of the flow depth from the bed in the vicinity of the inner bank to 10% the channel width away from the inner bank. With the relative curvature radius changed from 2 to 4, it was observed that the flow turbulence in front of the outer bank and at the water surface was lessened, and the vortex at the inner bank shrank (Fig. 8 (b)). With the piers installed streamwise to the flow direction and R=2B, a clockwise vortex was created in the vicinity of the inner bank. This vortex was extended to the level of 30% of the flow depth. In addition, a very small and weak vortex, highlighted with a red line in the figure, was generated between the two piers at a distance of 50% of the channel width at the level of approximately 25 to 35% of the flow depth. However, with an increase in the relative curvature radius and the channel bend becoming mild, the second secondary vortex which was developed in the vicinity of the outer bank and near the bed lost its power, the fact which became more evident with the piers installed in a streamwise position rather than those in a transverce position (Fig. 8 (c) and (d)).

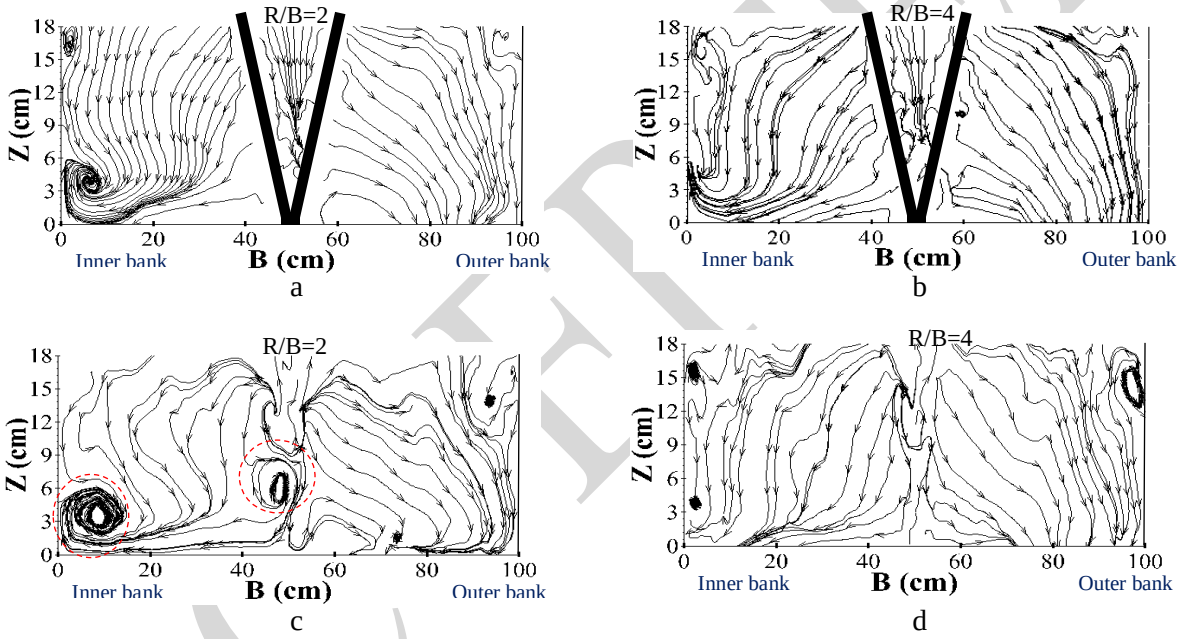

Fig. 8. An instance of the streamlines at cross sections crossing the center of the pier group, with the piers installed on a plane a) transverce and b) streamwise (c and d) to the flow direction at the 90° position with R=2, 4B.

As shown in Fig. 9 (a), a vortex was generated at the level of 22% from the bed; however, with the bend becoming mild (Fig. 9 (b)), it was observed that the center of this vortex was displaced to a distance equivalent to 2.5% the channel width away from the inner bank towards the water surface, and the second vortex at the same section was generated within 97% of the channel width away from the inner bank, and 85% of the flow depth away from the bed.

Material and predominant vortices of this section (Fig. 9(c)) appeared in two zones: the first zone near the inner bank close to the bed, and the second one near the pier 52% the channel width from the inner bank away. The vortex near the pier distanced from the bed by approximately 70.5 times the vortex at the inner bank and rotated in the opposite direction of the mainstream. After changing the relative curvature radius from 2 to 4 (Fig. 9 (d)), it was observed that this vortex did not directly attack the channel bed, and was in motion in a streamwise direction with the channel; therefore, it was driven upward after impacting the pier. Opposite to that, in the vicinity of the outer bank at a distance of 85% of the channel width from the inner bank, a vortex was observed with a streamwise direction at the level equal to 33 to 80% of the flow depth from the bed. This vortex was created as a result of generation of a return flow due to presence of the bridge pier. A comparison

between Figs. 7, 8, and 9 revealed that the milder the bend was, the smaller and less powerful the vortices became at the 120° position near the inner bank and the bed; nevertheless, this reduction in the power of the vortices was less than that in the other two positions of the piers.

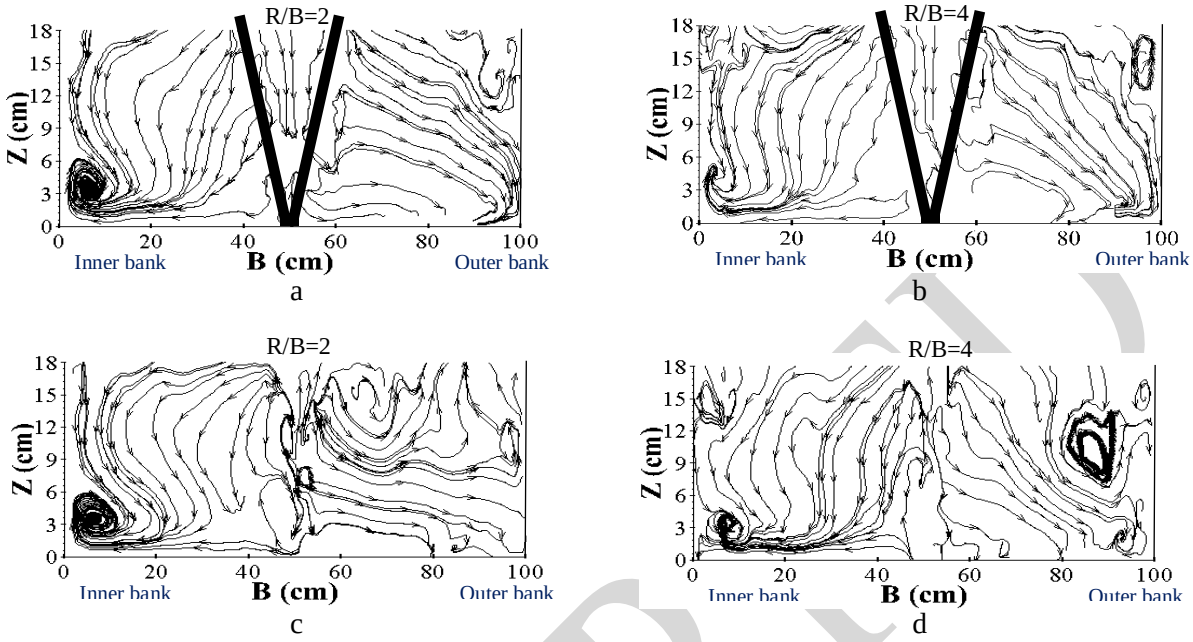

Fig. 9. An instance of the streamlines at the cross section crossing the center of the pier group, with the piers installed on a plane a) transverce and b) streamwise (c and d) to the flow direction at the 120° position with R=2, 4B.

Figs. 10 and 11 present an instance of the longitudinal sections of the streamlines for the models where the pier was installed at the 60° position either transverce or streamwise to the flow direction. Since the longitudinal sections were a result of the tangential and vertical velocities, and given the significantly higher value of the tangential velocity compared to the vertical velocity, the streamlines occurred at sections at a large distance from the pier in an approximately streamwise fashion.

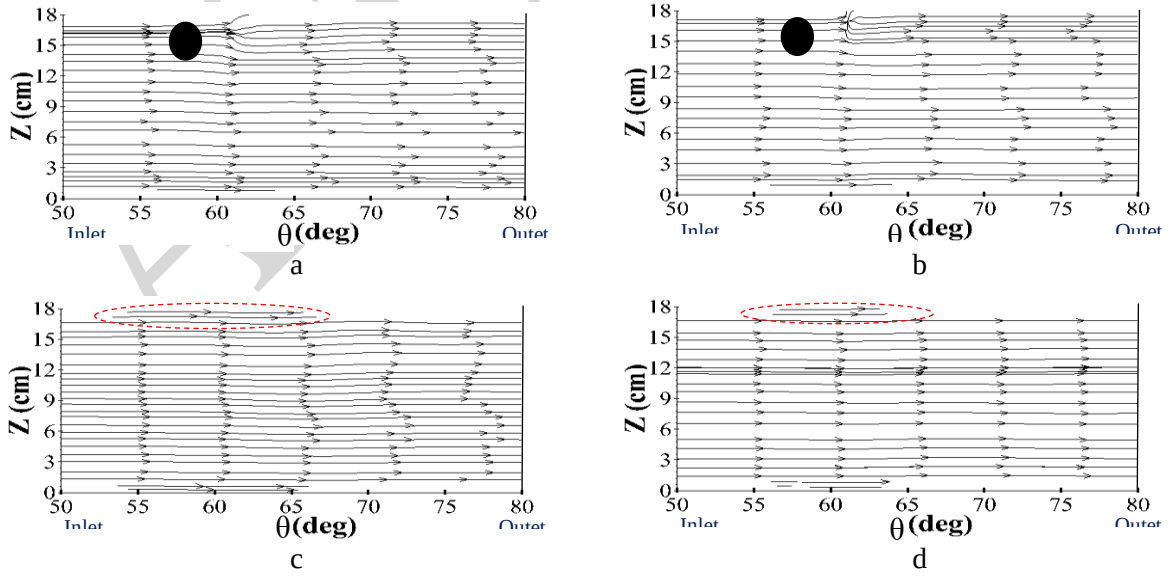

Fig. 10. A magnification of the streamlines at the longitudinal section at a distance of 40% of the channel width from the inner bank with the piers installed on a plane a) transverce and b) streamwise (c and d) to the flow direction at the 60° position with R=2, 4B.

According to Fig. 10 (a) and (b), it may be noted that after impacting the pier, the flow was deviated upward and downward, and then again extended in a straight direction along the bend. Flow deviation was due to the effect of down flows after collision with the bridge pier structure, which was installed transverce to the flow direction. This flow was deviated along the path after an impact with longitudinal flows. Collision of the streamlines occurred at the downstream side of the piers with the flow passing by the piers in the sharp bend. This point at R=2B was located near the water surface, and with the bend becoming milder, this separation and proximity of the flow was lessened. With the piers installed on the plane streamwise with the flow direction, as in Fig. 10 (c) and (d), it may be observed that the streams near the bed at the site of the piers were not steady, but turbulent, and the flow was slightly deviated upward around the piers. It was also evident near the water surface that the flows deviated upward after impacting the piers, and the flow depth at this zone was higher than that of the other sections of the bend. The range of such alterations in water level was smaller in the mild bend than that in the sharp bend. The streams at the downstream side of the piers were completely steady and calm.

The same holds true for the longitudinal section at a distance of 60% of the channel width from the inner bank (Fig. 11).

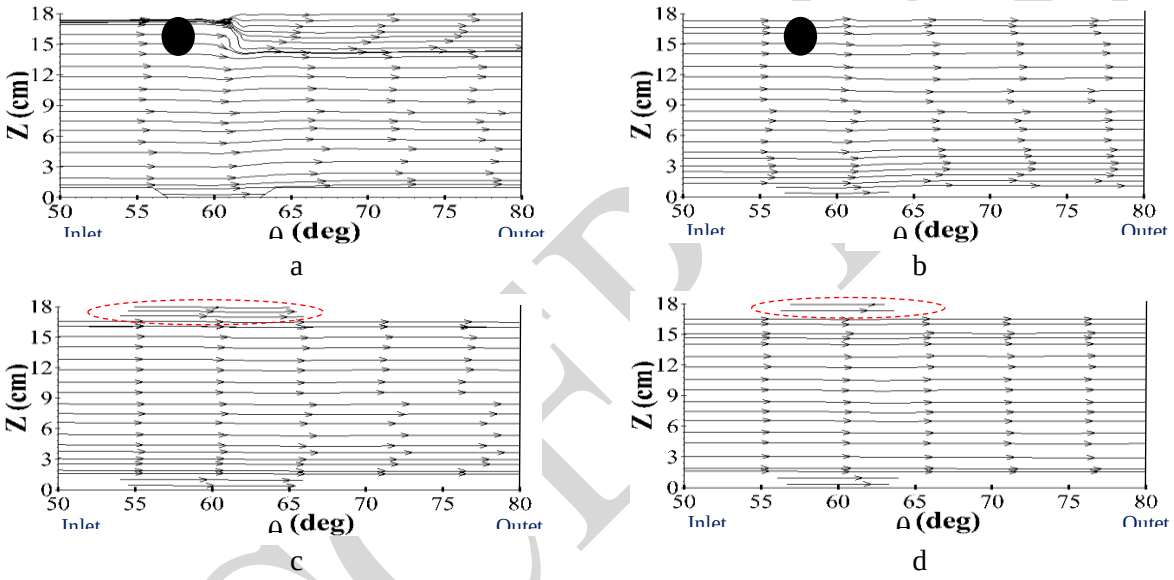

Fig. 11. A magnification of the streamlines at the longitudinal section at a distance of 60% of the channel width from the inner bank with installation of the piers on a plane a) transverce and b) streamwise (c and d) to the flow direction at the 60° position with R=2, 4B.

Figs. 12 and 13 display an example of the streamlines at plan section at 5 and 95% of the depth along with magnified views of the flows developed at the piers, so that more precise and high quality examination of the flows around the bridge pier could be achieved. The series of V-shaped piers presented in these pictures are positioned at the 90° location. As shown by Fig 12 (a) and (b), the streamlines are separated closer to the vicinity of the piers, and the flow separation zone vividly appears upstream of the piers. This refers to the fact that the effect of the presence of hydraulic structures in the bend is a local effect. Furthermore, after passing by the piers, the streams rearrange and follow their path towards the curve of the bend. This flow separation is less significant with a lower curvature radius; with a greater curvature radius, and the bend becoming milder, such a deviation in the streamlines around the pier group is less significant. Furthermore, it may be observed that the streamlines with R=2B oriented towards the inner bank far more than those with R=4B. Additionally, with piers installed on a plane streamwise to the flow direction (Fig. 12 (c) and (d)), it may be observed that the streamlines in the vicinity of the piers deviated from their path. When R=4B, with a milder bend, the streams were not significantly deviated around the piers. The flow separation zone with the piers installed streamwise with the flow direction was smaller than that with piers in a transverce position. This was particularly observed in extended bends with R=4B.

The centrifugal force inside the bend resulted in a higher water level at the outer bank and a lower water level at the inner bank. Consequently, with the pressure gradient taken into consideration at higher levels, Fig.

13, the streamlines near the water surface were oriented towards the outer bank. If the outer bank wall is erodible, erosion due to flow attacking the outer bank is expected to occur at higher levels of the flow. As shown in the figure, the streamlines deviated towards the outer bank in the first half of the bend, and then they were aligned with the bend in the second half. The flow separation also continued to a short distance at the downstream side of the piers at this level. With a comparison between the plans of different bends in the mentioned figures, it may be revealed that the streamlines at the water surface attacked and collided with the banks with a greater deviation in the sharp bend with R=2B. A comparison between Figs. 12 and 13 indicates that the flow separation zone behind the piers was extended further at higher levels.

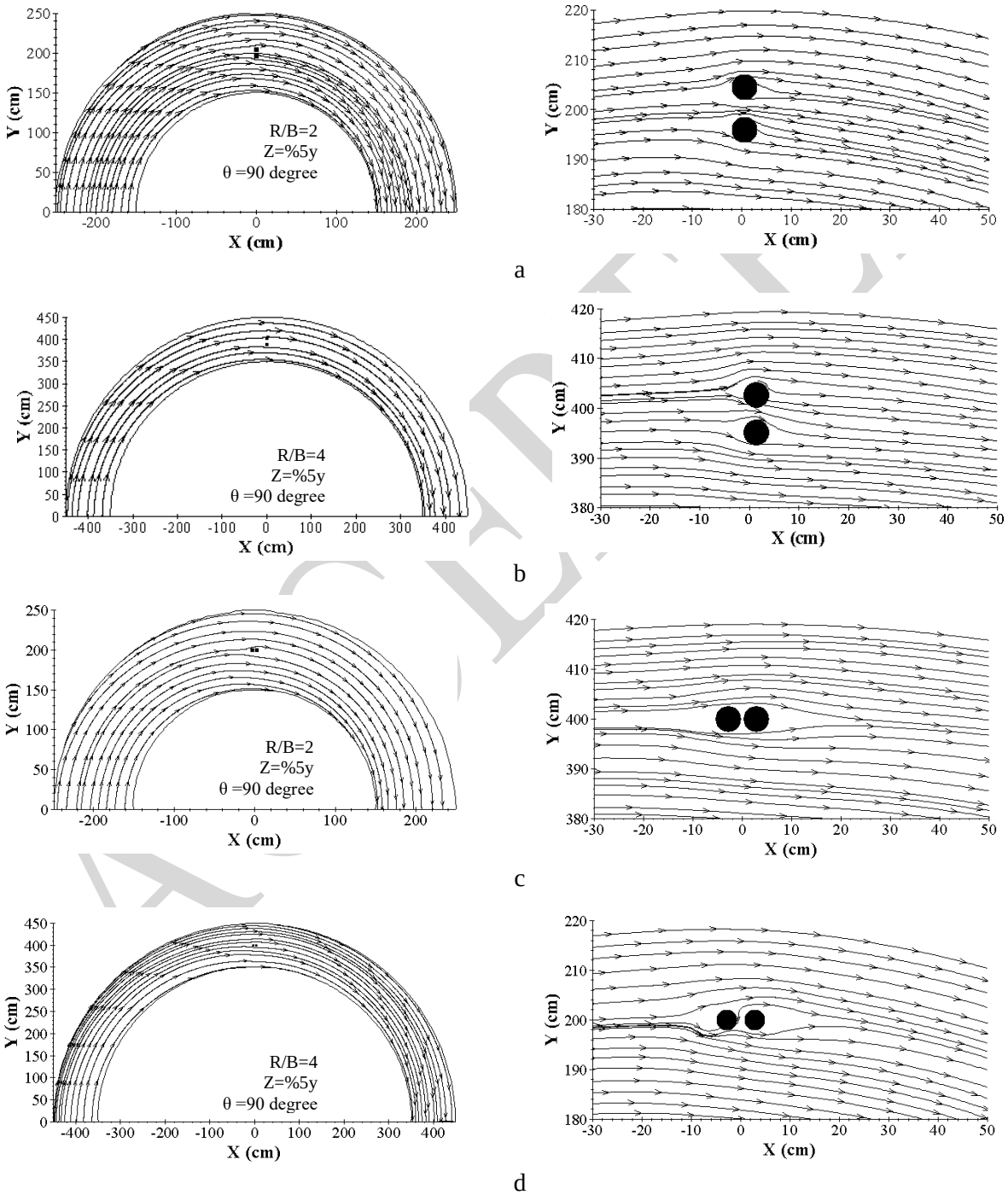

Fig. 12. An instance of the streamlines at the level of 5% of the flow depth from the bed with the piers installed on a plane a) transverce and b) streamwise (c and d) to the flow direction at the 90° position with R=2, 4B.

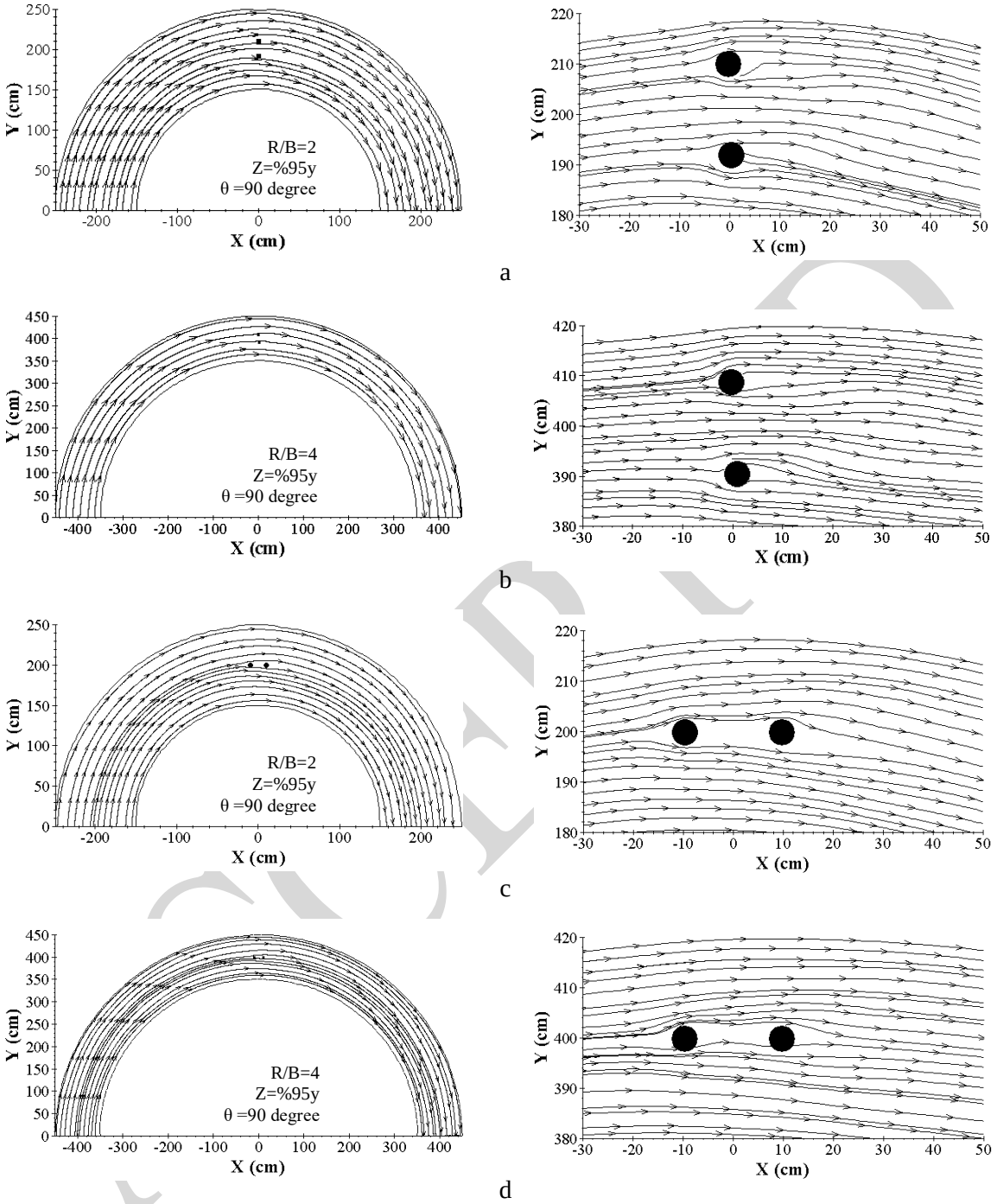

Fig. 13. An instance of the streamlines at the level of 95% of the flow depth from the bed with the piers installed on a plane a) transverce and b) streamwise (c and d) to the flow direction at the 90° position with R=2, 4B.

Figs. 14 and 15 depict an instance of tangential velocity contours at different plan sections at levels of 5 and 95% of the flow depth from the bed with the piers installed at the 120° section from the bend entrance either transverce or streamwise to the flow direction. Fig. 14 (a) and (b) illustrate the tangential velocity contour at the level near the bed with the piers installed on a plane transverce to the flow direction. At most points of this level, the tangential velocity was positive (oriented towards the bend end with a streamwise direction), and it was negative only around the piers. The maximum negative and positive tangential velocities decreased by 12.5 and 5% respectively with a 2 to 4 increase in the relative radius of curvature.

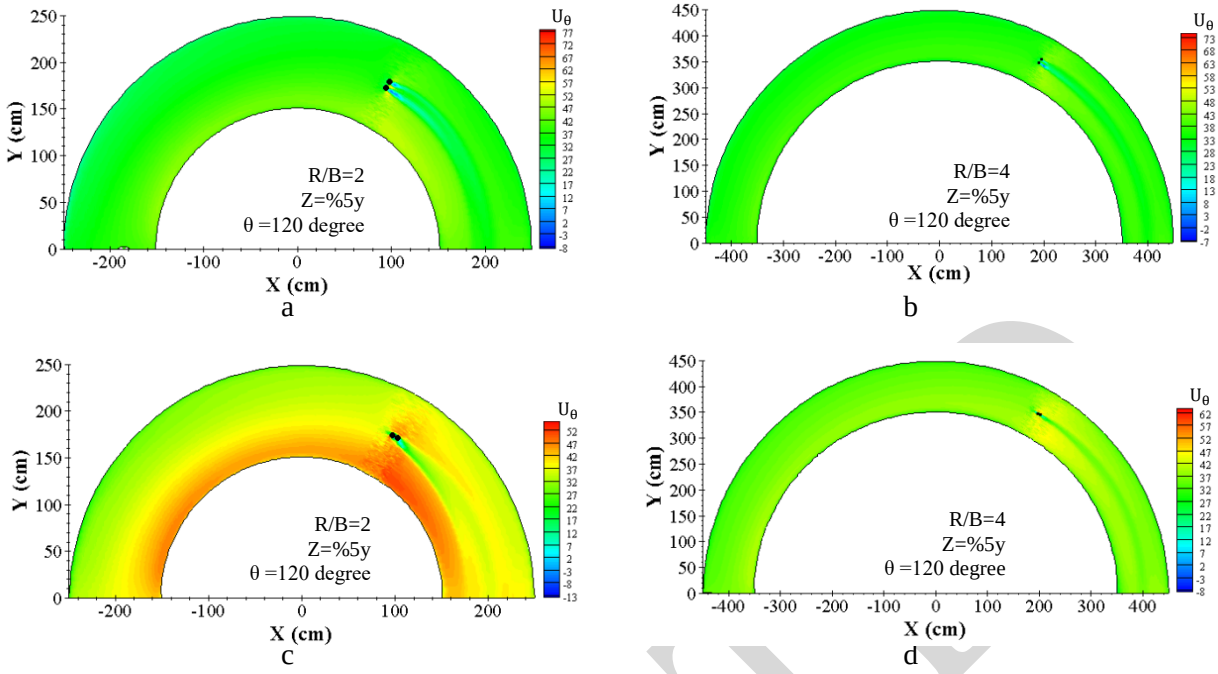

Fig. 14. Tangential velocity contours at a level equal to 5% of the flow depth from the bed with the piers installed on a plane a) transverce and b) streamwise (c and d) to the flow direction at the 120° position with R=2, 4B.

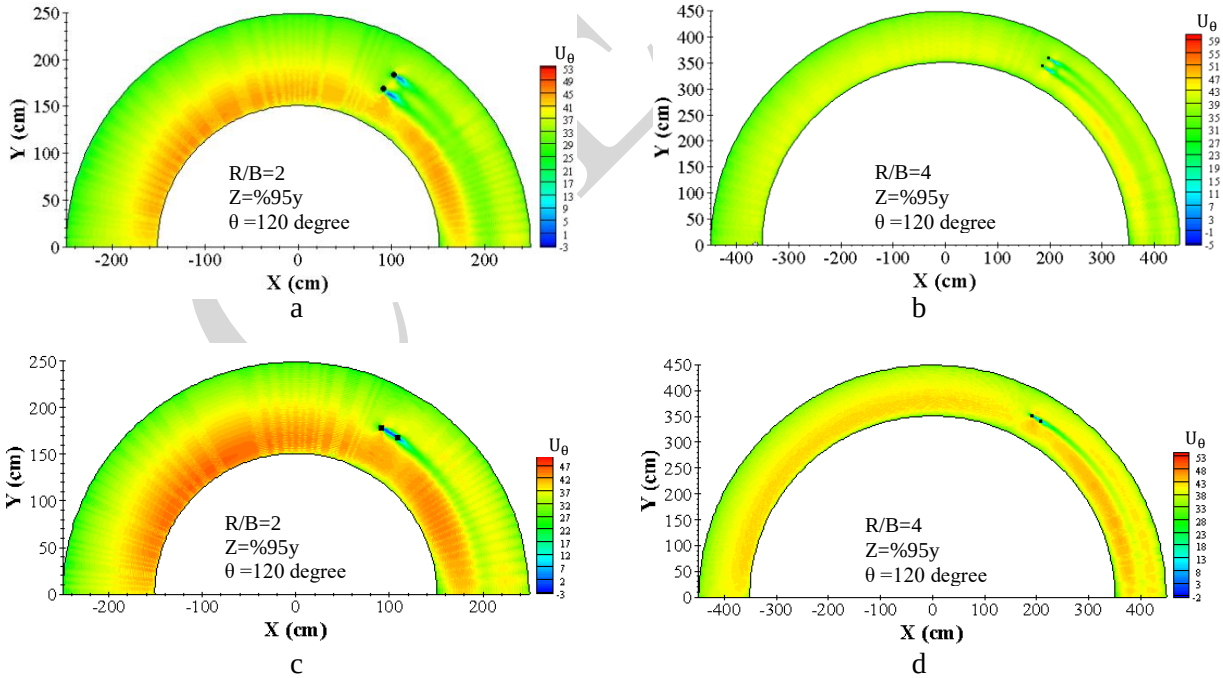

Fig. 15. Tangential velocity contours at a level equal to 95% of the flow depth from the bed with the piers installed on a plane a) transverce and b) streamwise (c and d) to the flow direction at the 120° position with R=2, 4B.

The maximum negative and positive values of tangential velocity underwent 12.5 and 5% declines respectively after changing the relative radius of curvature from 2 to 4, while streamwise installation of the piers to the flow direction (Fig. 14 (c) and (d)) and increasing the relative curvature radius increased the maximum positive tangential velocity by 16.10%. Fig. 16 shows that at a higher level, the positive and negative

tangential velocity values, as well as the turbulences, decrease due to their distance from the bed (Fig. 14). It is evident with transverce installation of the piers to the flow direction (Fig. 15 (a) and (b)) and the bend becoming milder that the field and the power of return flows decreased around the piers. As observed in Fig. 15 (c) and (d), a 2 to 4 increase in the relative curvature radius increased the maximum positive tangential velocity by 13%, while the maximum negative tangential velocity decreased by approximately 33%.

Figs. 16 and 17 display the geometric situation of the line of the maximum flow velocity at varous levels regarding the series of V-shaped piers implemented at the 60, 90, and 120° locations on a transverce or streamwise plane with R=2 and 4B at 5 and 95% the depth from the bed. It may be observed in Fig. 16 that when the flow entered the sharp bend, because of the pressure gradient resulting from the centrifugal force, the maximum velocity at the initial sections of the sharp bend occurred towards the inner bank at the level near the bed, and in the case of the mild bend, it occurred on the central line of the bend, and accelerated water particles. On the other hand, at the bend's end, the longitudinal pressure gradient was negative along the outer bank, and it was positive along the inner bank.

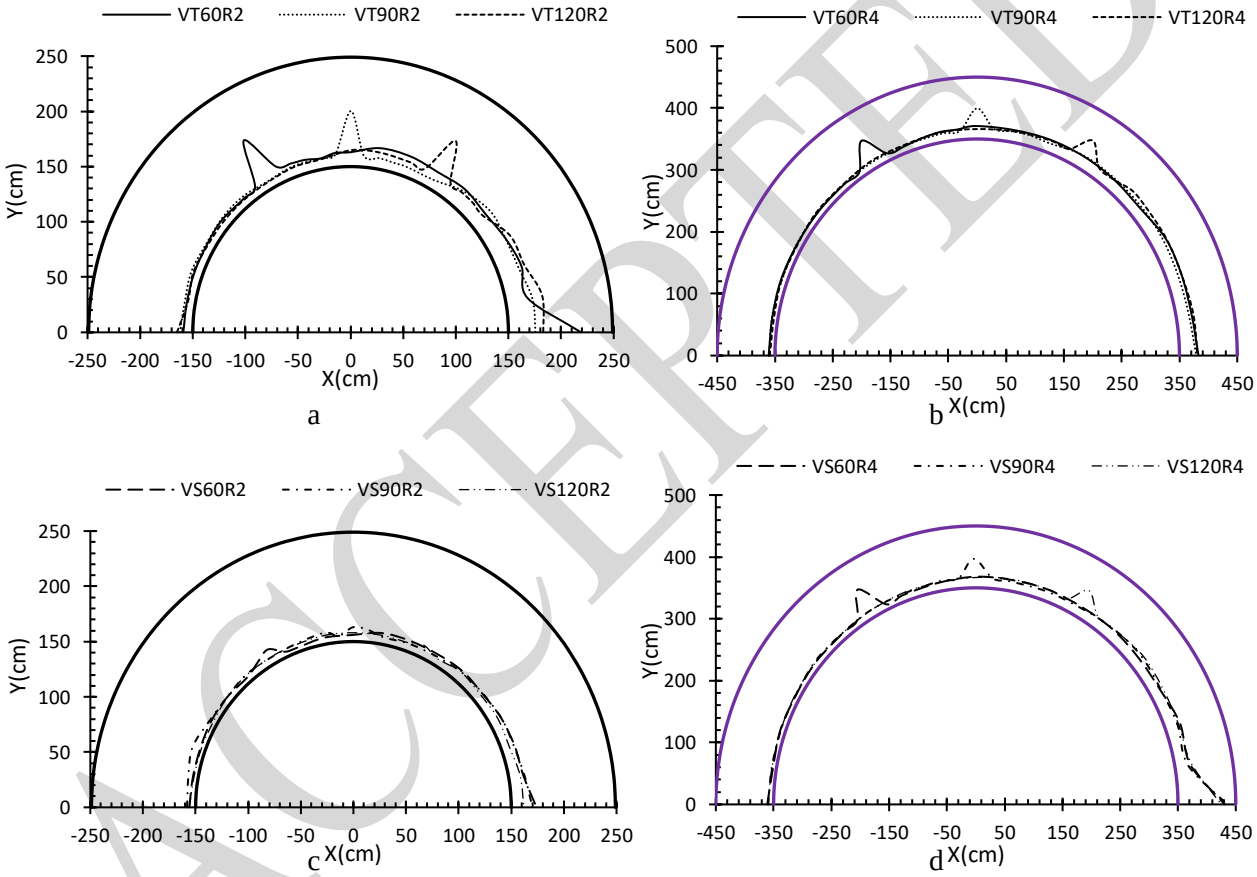

Fig. 16. The maximum velocity path along the bend at a level equal to 5% of the flow depth from the bed with the piers installed on a plane a) transverce and b) streamwise (c and d) to the flow direction with R=2, 4B.

Interference of the negative longitudinal gradient and the secondary flow at this section raised velocity. Hence, the maximum velocity in both sharp and mild bends occurred towards the outer bank. As a consequence, in the sharp bend, the highest distance of the geometric location of the maximum velocity lines at the bend's end from the inner bank, 70% of the channel width from the inner bank, occurred in VT60R2 model. Furthermore, in the vicinity of the pier in the sharp bend, the maximum velocity further deviated towards the site of the piers. Whereas, in the mild bend, there was less deviation of this flow path observed in the vicinity of the piers (Fig. 16 (a) and (b)). After altering the position of the piers from transverce to streamwise to the flow direction, the geometric location of the maximum velocity around the piers decreased in the sharp bend, and unexpectedly increased in the mild bend.

In the sharp bend, the maximum velocity line followed a milder path towards the water surface than 5% of the depth from the bed, while the same tendency in the mild bend occurred in a totally opposite direction, and the line of the maximum flow velocity at the level in proximity of the bed was on a milder slope. The greatest range of geometric situation of the maximum velocity lines within the sharp bend at the end of the bend from the inner bank appeared in VT60R2 model as 50% the channel width away from the inner bank; however, with the mild bend, it took place at 40% the channel width away from the inner bank for every model (Fig. 17 (a) and (b)). When the piers were repositioned from transverce to streamwise, the distance of the maximum velocity line at the end of the bend from the inner bank declined in the sharp bend, and rose in the mild bend; afterwards, it happened at 80% the channel width away from the inner bank in VS90R4 model (Fig. 17 (c) and (d)).

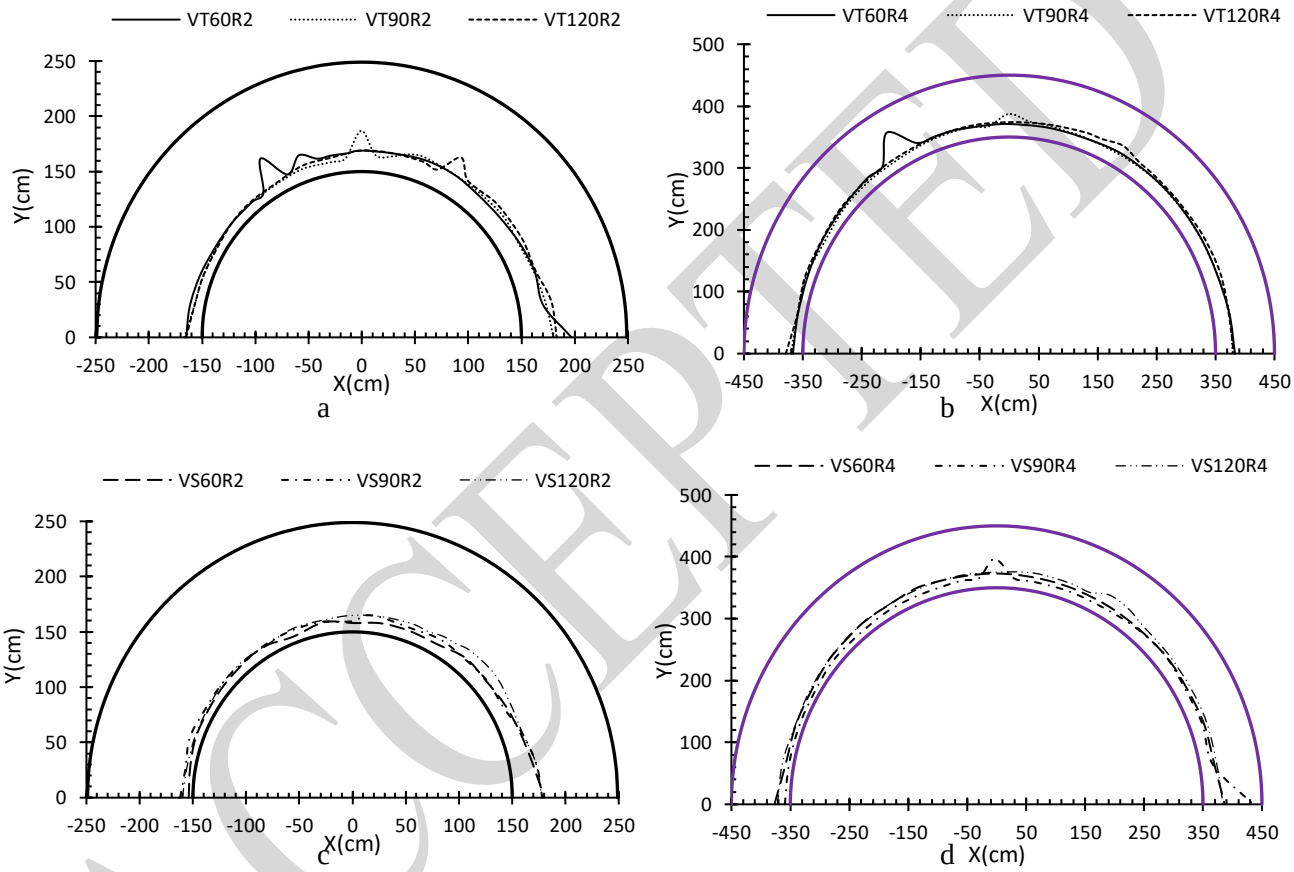

Fig. 17. The maximum velocity path along the bend at a level equal to 95% of the flow depth from the bed with piers installed on a plane a) transverce and b) streamwise (c and d) to the flow direction with R=2, 4B.

The secondary flow dominant in the bends and the interplay between the secondary flow and the longitudinal flow led to generation of a helical flow within the bend. Indeed, the secondary flow strength referred to the robustness of the lateral sediment displacement. Hence, with the aim of predicting the scour pattern, which is the main aim of flow pattern models, the secondary flow power along the bend was calculated. There are a variety of criteria for determining the secondary flow power. The first criterion is the vorticity criterion, also known as velocity curl, and its equations are presented as follows [35].

$$\omega = \frac{1}{2}\left(\frac{\delta v}{\delta z} - \frac{\delta w}{\delta r}\right) \quad (5)$$

where V and W represent the mean radial and vertical velocity components.

Fig. 18 (a) presents vorticity values calculated for installation of the V-shaped pier group at the 60° position per relative curvature radii of 2, 3, 4, and 5 with two installations of the piers. As shown in the figure, vorticity increased towards the vicinity of the piers, where the maximum value equal to 14.7 per second occurred in VT60R3 model. With installation of the piers at the 90° position transverce to the flow direction, the value of

this parameter was in a negative correlation with the increase in the relative curvature radius; at relative curvature radii of R/B=2, 3, 4, and 5, its value was respectively 7.87, 7.79, 7.67, and 6.88 (Fig. 18 (b)). With the piers installed at the 120° position (Fig. 18 (c)), the maximum vorticity occurred in VT120R2 for 13.9 per second. Furthermore, the minimum vorticity value, 5 per second, occurred in VS120R5 model. The maximum vorticity was 2.8 times the minimum. Although the maximum vorticity occurred with piers installed transverce to the flow direction, the range and reach of this rotation in these models were smaller than those in models where the piers were installed streamwise to the flow direction. It may be observed in Fig. 19 that the amount of vorticity at the downstream side of the piers significantly decreased in every case, and its variations were of little significance to the end of the bend. A comparison of vorticity in case of piers installed transverce to the flow direction and that in case of piers installed streamwise to the flow direction indicates that vorticities at the 60° and 120° positions were larger than their corresponding values at the 90° position.

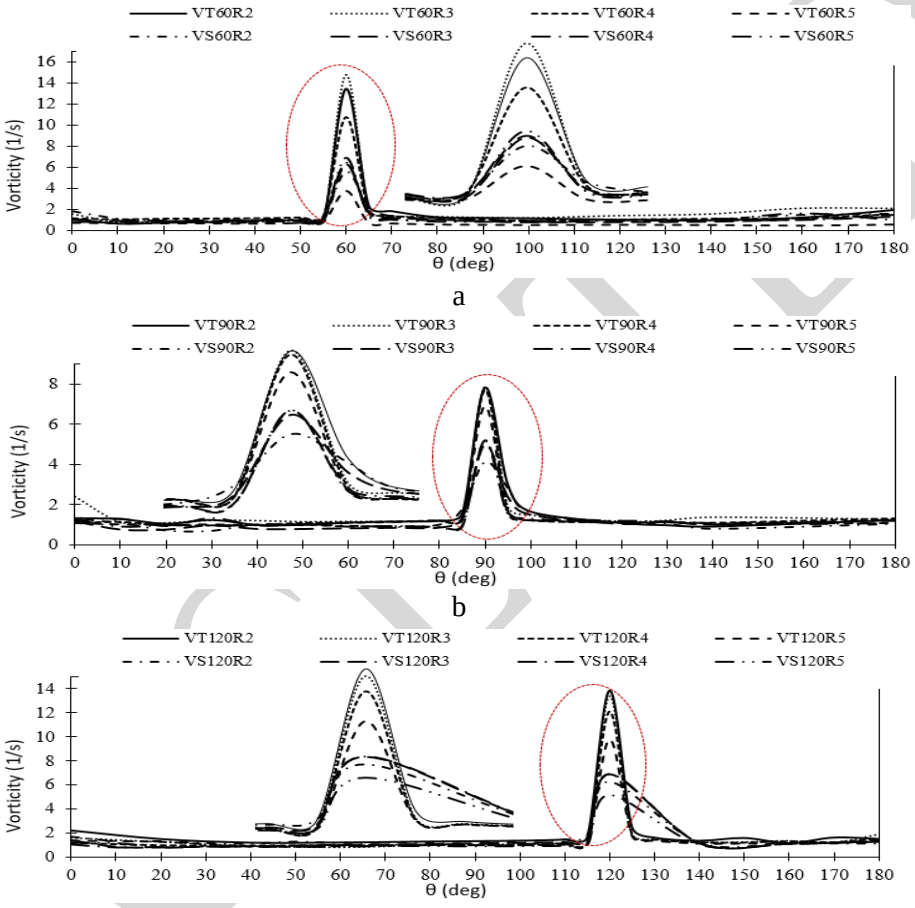

Fig. 18. An illustration of vorticity alterations throughout the bend with a magnification of the area around the piers in models with the bridge piers installed at a) 60, b) 90, and c) 120° positions from the bend entrance.

The next standard considered in calculating the secondary flow strength was the Shukry criterion. Shukry (1950) examined the flow in meandering paths and also described the secondary flow process. In order to discuss this case for the secondary flow, the following criteria were proposed [36].

$$Sxy = \frac{k_{lateral}}{k_{main}}\left(\frac{v^2+w^2}{u^2+v^2+w^2}\right) \quad (6)$$

Here, S_{xy} refers to the power of the secondary flow, $K_{lateral}$ and K_{main} respectively denote the lateral-flow kinetic energy and the mainstream kinetic energy, and u, v and w show the components of velocity along respectively x, y, and z.

The secondary flow power at different cross sections was calculated through this criterion, which is shown in Fig. 19 for both positions of the piers with respect to the flow direction. It is noted that the effect of installation of the piers in a streamwise direction on the quantitative value of the secondary flow power is

evident. At different relative radii, the maximum secondary flow power occurred in the vicinity of the piers. This is observed with installation of the V-shaped piers at 60, 90 and 120° positions in either transverce or streamwise directions with the flow, the fact which may be attributed to the down flows at the pier nose and the increase in the radial component. Even though this pattern was modeled under rigid bed conditions, it helped understand the location of the hole around the piers and the scour along the bend. Given the maximum values of the secondary flow power, the maximum scour was expected to occur in this zone in the bend. Fig. 19 (a) shows that the maximum secondary flow power of the second kind occurred in VS60R4 model at an approximate value of 18.8%. Furthermore, in the model with R=2B, when the pier was installed transverce to the flow direction, the secondary flow power reached minimum. The ratio of the maximum secondary flow power to its minimum in two models with R=2, 4B was equal to 2.6. The maximum and minimum values of the secondary flow power under this circumstances decreased by installing the pier in a transverce direction with the flow.

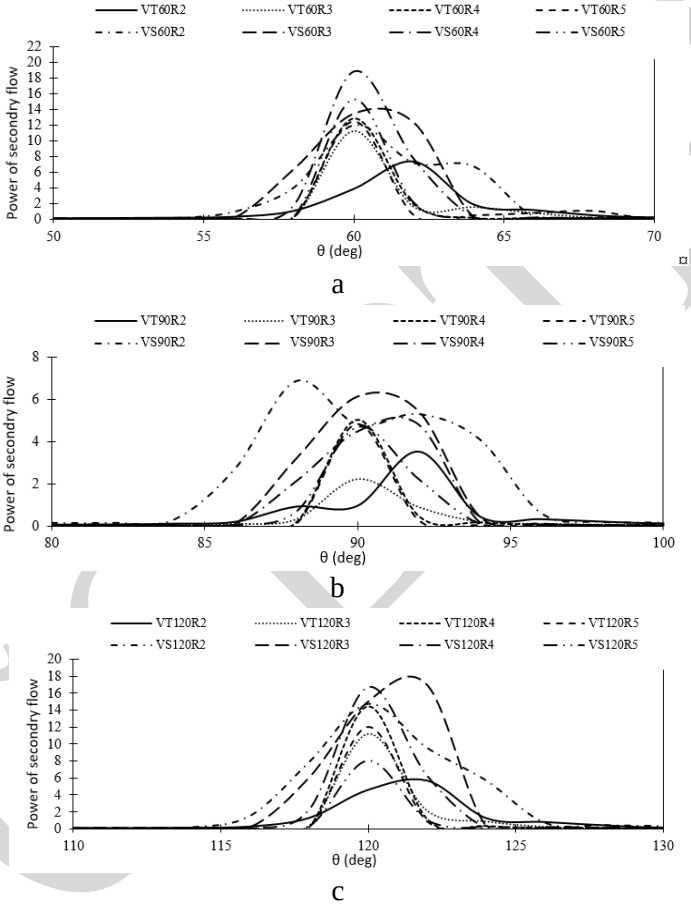

Fig. 19. A view of the secondary flow power variations at the area around the piers in models with bridge piers installed at a) 60, b) 90, and c) 120° positions from the bend entrance.

According to Fig. 19 (b), with the piers installed transverce to the flow direction, it may be stated that under mobile bed conditions, the range of the scour hole around the pier was larger in a sharp bend than that in extended bends; the scour hole at the pier in a sharp bend developed in a range around 4 times the pier diameter in upstream and downstream directions; however, that in extended bends covered a distance of twice the pier diameter. It may also be observed that the secondary flow value in VS90R2 model was higher than that in the other models with a maximum of 6.8% at the 88° position. As shown in the figure, with a curvature radius of 2 in the vicinity of the piers, the secondary flow power decreased between the two piers and finally increased immediately after the location of the pier. Additionally, with the piers installed streamwise to the flow direction, the minimum secondary flow power occurred in VS60R4 model for 4.6%, while with the piers installed on a plane transverce to the flow direction at this position, the maximum and the minimum values of this parameter occurred respectively in VT90R3 and VT90R4 by 2.2 and 5%. With installation of the V-shaped pier group on a plane streamwise to the flow at the 120° position, according to Fig. 19 (c), it may be observed

that the maximum and the minimum secondary flow power values occurred in VS120R3 and VT90R4 for respectively 16.9 and 8.09%. In every three position of the piers as transverce to the flow direction, the maximum values of the secondary flow power with R=2B was found behind the pier, while with other curvature radii, this parameter was maximum at the site of the piers. As depicted in the figure, away from the site of the piers, the secondary flow power values significantly decreased with all 4 relative curvature radii. It could be argued that section constriction occurred in the vicinity of the piers, and the flow velocity increased in these zones.

The flow deviation consisted of the average horizontal angle of the streamlines at a certain section, and was denoted by α. Fig. 20 illustrates measurement of the flow angle of deviation. Positive values of α indicated the streamlines deviation in a counterclockwise direction.

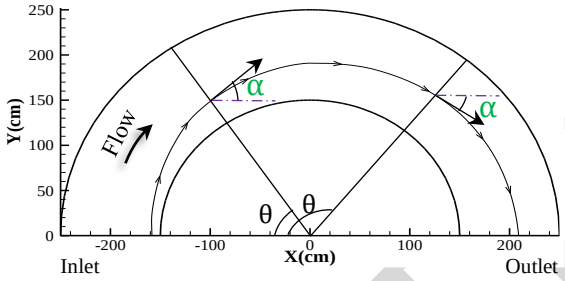

Fig. 20. Measurement of the streamlines' angle of deviation.

Table 3 presents an instance of the streamlines' angles of deviation with the V-shaped piers located at the 60° position in a bend with R=2, 4B. As suggested by the table, the values of the angle of deviation were positive in the first half of the bend and then became negative in the second half.

Table 3. The streamlines angles of deviation.

Row	θ(deg)	VT60R2		VT60R4		VS60R2		VS60R4	
		5%y	95%y	5%y	95%y	5%y	95%y	5%y	95%y
1	0	86.35	86.65	88.27	87.26	87.69	88.56	88.27	88.19
2	10	76.92	78.89	78.67	79.61	80.87	79.37	78.83	79.47
3	20	66.28	69.99	68.04	70.17	72.31	70.27	68.08	69.98
4	30	55.57	60.27	57.26	60.44	61.49	60.03	57.19	60.22
5	40	45.00	50.17	46.84	50.14	50.22	50.07	46.69	50.06
6	50	34.80	40.17	36.87	40.12	39.50	40.26	36.73	40.02
7	55	30.03	35.35	31.93	35.09	34.11	35.48	31.82	35.00
8	60	27.60	31.95	23.26	28.64	20.62	29.93	37.63	29.01
9	65	23.71	23.93	23.59	24.67	25.61	25.06	24.76	24.93
10	70	17.94	19.78	18.29	20.55	21.03	20.24	19.15	20.45
11	75	12.30	15.32	13.13	15.60	15.99	15.70	13.77	15.76
12	80	6.85	10.77	7.92	10.72	10.55	10.84	8.36	10.51
13	90	-4.05	1.01	-2.13	0.46	-0.35	1.11	-2.00	0.21
14	100	-14.53	-9.09	-12.12	-9.81	-11.35	-9.73	-12.29	-9.98
15	120	-35.16	-29.91	-32.49	-30.26	-32.01	-31.20	-32.75	-30.47
16	140	-54.82	-50.30	-52.31	-50.73	-51.44	-51.02	-52.37	-50.78
17	160	-74.78	-69.99	-72.30	-71.19	-71.51	-70.44	-72.29	-70.86
18	180	-89.40	-86.56	-89.98	-87.75	-87.40	-85.34	-89.69	-87.92

In general, at the bend entrance, the angles of deviation at both levels were almost equal, equal to the horizontal angle of 90°. Along the bend, this parameter was reduced at all levels; it reached zero at the bend apex (at the 90° section), became negative in the second half of the bend, and turned into approximately -90 at the end of the bend at both levels. It is also suggested that the curves on the levels near the water surface for every

installation of the bridge piers were higher than the curves on the level near the bed, the fact which referred to the streamlines' deviation towards the outer bank at water surface. The lower height of the curve on the level near the bed was indicative of the streamlines' deviation towards the inner bank. An exception could also be noted here: it was observed in VS60R4 model that the angle of deviation near the bed was approximately 8.5° larger than that near the water surface in the vicinity of the pier. Further, the maximum difference in the angles of deviation between the level near the bed and that near the water surface at the site of the piers occurred in VS60R2 model for 9.3°.

5 Conclusion

This paper investigated the flow pattern and 3D velocities by repositioning pairs of V-shaped piers in streamwise and transverce directions with water flowing inside a 180°bend with different relative curvature radii under rigid bed conditions. The results of this research are presented in the range of variations in parameters as follows:

The numerical and experimental results of the flow pattern matched appropriately under rigid bed conditions, the fact which refers to the great capability of ANSYS numerical model in determining the flow pattern in bent channels containing inclined bridge piers.

After impacting the pier, the flow was first deviated upward and downward and then it was extended in a straight path along the bend. The deviation was due to the effect of down flows after impact with the bridge pier structure perpendicular to the flow direction. This flow was deviated along the path after impacting the longitudinal flows. After the flow passed the piers in the sharp bend, the streamlines intersected at the piers' downstream side. The point of intersection with R=2B was located near the water surface, and use of a milder bend reduced flow separation and approximation.

The streamlines separated as they approached the piers site, and the flow separation was clearly apparent upstream of the pier, which indicates the local effect of hydraulic structures present at the bend. Further, after the streams passed by the piers, they continued along the bend curve from the downstream side of the piers. This flow separation was more significant at the smaller curvature radius, while increasing the curvature radius and making the bend milder made the separation around the pier group less significant.

The changes in the secondary flow strength and vorticity within the bend had nearly similar mechanisms. The maximum value of these two parameters occurred considering the rigid bed at the site of the piers. The maximum value of the secondary flow power was 18.8% and the maximum vorticity was 14.7 per second, respectively occurring in VS60R4 and VT60R3 models.

The vorticity values at the 60 and 120° positions were larger than their corresponding values at the 90° position.

It was observed in every model that at any level near the bed and near the water surface, when the flow reached the piers, flow separation occurred and the streams approached each other at the downstream side of the pier. However, increasing the relative curvature radius reduced the amount of separation and approximation.

The flow separation zone with the piers installed streamwise to the flow direction was smaller than that with the piers installed in a transverce direction. This was particularly and clearly observed with the relative curvature radius of 4.

References

[1]. Mendoza-Cabrales C (1993) Computation of flow past a cylinder mounted on a flat plate. In Hydraulic Engineering, pp 899-904.

[2]. Rodi W (1997) Comparison of LES and RANS calculations of the flow around bluff bodies. Journal of wind engineering and industrial aerodynamics, 69:55-75. DOI: 10.1016/s0167-6105(97)00147-5

[3]. Richardson J.E, Panchang V.G (1998) Three dimensional simulation of scour inducing flow at bridge piers. Journal of Hydraulic Engineering, 124(5):530-540. DOI: 10.1061/(asce)0733-9429(1998)124:5(530)

[4]. Yen C.L, Lai J.S, Chang W.Y (2001) Modeling of 3D flow and scouring around circular piers. Proceedings of the National Science Council, Republic of China. Part A, Physical science and engineering, 25(1):17-26.
[5]. Graf W.H, Istiarto I (2002) Flow pattern in the scour hole around cylinder. Journal of Hydraulic Research, 40(1):13-20. DOI: 10.1080/00221680209499869
[6]. Ali K.H, Karim O (2002) Simulation of flow around piers. Journal of Hydraulic Research, 40(2):161-174. DOI:10.1080/00221680209499859
[7]. Salaheldin T.M, Imran J, Chaudhry M.H (2004) Numerical modeling of three-dimensional flow field around circular piers. Journal of Hydraulic Engineering, 130(2):91-100. DOI: 10.1061/(asce)0733-9429(2004)130:2(91)
[8]. Ettema R, Kirkil G, Muste M (2006) Similitude of large-scale turbulence in experiments on local scour at cylinders. Journal of Hydraulic Engineering, 132(1):33-40. DOI: 10.1061/(asce)0733-9429(2006)132:1(33)
[9]. Beheshti A.A, Ataie-Ashtiani B (2009) Experimental study of three-dimensional flow field around a complex bridge pier. Journal of engineering mechanics, 136(2):143-154. DOI:10.1061/(asce)em.1943-7889.0000073
[10]. Das D, Das R, Mazumdar A (2013) Circulation characteristics of horseshoe vortex in scour region around circular piers. Water science and engineering, 6(1):59-77. DOI: 10.3882/j.issn.1674-2370.2013.01.005
[11]. Vaghefi M, Ahmadi A, Faraji B (2015) The effect of support structure on flow patterns around T-shape spur dike in 90 bend channel. Arabian Journal for Science and Engineering, 40(5):1299-1307. DOI: 10.1007/s13369-015-1604-2
[12]. Ehteram M, Meymand A.M (2015) Numerical modeling of scour depth at side piers of the bridge. Journal of Computational and Applied Mathematics, 280:68-79. DOI: 10.1016/j.cam.2014.11.039
[13]. Hamidi A, Siadatmousavi S.M (2017) Numerical simulation of scour and flow field for different arrangements of two piers using SSIIM model. Ain Shams Engineering Journal, 13.9(4):2415-2426. DOI:10.1016/j.asej.2017.03.012
[14]. Asadollahi M, Vaghefi M, Akbari M (2020) Effect of the position of perpendicular pier groups in a sharp bend on flow and scour patterns: numerical simulation. Journal of the Brazilian Society of Mechanical Sciences and Engineering, 42(8):1-15. https://doi.org/10.1007/s40430-020-02503-2
[15]. Vaghefi M, Ghodsian M, Salimi S (2016) Scour formation due to laterally inclined circular pier. Arabian Journal for Science and Engineering, 41(4):1311-1318. DOI: 10.1007/s13369-015-1920-6
[16]. Wang H, Tang H, Liu Q, Wang Y (2016) Local scouring around twin bridge piers in open-channel flows. Journal of Hydraulic Engineering, 142(9):6001-6008. DOI: 10.1061/(asce)hy.1943-7900.0001154
[17]. Khaple S, Hanmaiahgari P.R, Gaudio R, Dey S (2017) Interference of an upstream pier on local scour at downstream piers. Acta Geophysica, 65(1):29-46. DOI: 10.1007/s11600-017-0004-2
[18]. Vaghefi M, Tabib Nazhad Motlagh M. J, Hashemi S. Sh, Moradi S (2018) Experimental study of bed topography variations due to placement of a triad series of vertical piers at different positions in a 180° bend. Arabian Journal of Geosciences, 11(5):102. DOI: 10.1007/s12517-018-3443-4
[19]. Abdi Chooplou Ch, Vaghefi M (2019) Experimental Study of the Effect of Displacement of Vanes Submerged at Channel Width on Distribution of Velocity and Shear Stress in a 180 Degree Bend. Journal of Applied Fluid Mechanics, 12(5):1735-3645. DOI: 10.29252/jafm.12.05.29329
[20]. Safaripour N, Vaghefi M, Mahmoudi A (2020) Experimental study of the effect of submergence ratio of double submerged vanes on topography alterations and temporal evaluation of the maximum scour in a 180-degree bend with a bridge pier group. *International Journal of River Basin Management*, 1-15. https://doi.org/10.1080/15715124.2020.1837144
[21]. Vaghefi M, Solati S, Abdi Chooplou Ch (2021). The effect of upstream T-shaped spur dike on reducing the amount of scouring around downstream bridge pier located at a 180° sharp bend. *International Journal of River Basin Management*, *19*(3), 307-318. https://doi.org/10.1080/15715124.2020.1776306
[22]. Moghanloo M, Vaghefi M, Ghodsian M (2020) Experimental investigation on the Effect of Increasing the Collar Thickness on the Flow Pattern around the Oblong Pier in 180° Sharp Bend with Balanced Bed. Journal of Applied Fluid Mechanics, 13(1):245-260. https://doi.org/10.29252/jafm.13.01.30164
[23]. Sedighi F, Vaghefi M, Ahmadi G (2020) The effect of inclined pair piers on bed topography: clear water, incipient motion and live bed. Iran J Sci Technol Trans Civ Eng. https ://doi.org/10.1007/s4099 6-020-00481 -y

[24]. Dehghan D, Vaghefi M, Ghodsian M (2021) Experimental study of the effect of the length-to-width ratio and skewness angles of the pier installed at the bend on scour pattern. *Journal of the Brazilian Society of Mechanical Sciences and Engineering*, *43*(3):1-17. https://doi.org/10.1007/s40430-021-02884-y
[25]. Keshavarz A, Vaghefi M, Ahmadi G (2021). Effect of the Shape and Position of the Bridge Pier on the Bed Changes in the Sharp 180-Degree Bend. Iranian Journal of Science and Technology, Transactions of Civil Engineering, 1-19. https://doi.org/10.1007/s40996-021-00787-5
[26]. Solati S, Vaghefi M, Behroozi AM (2021) Effect of duration and pattern of hydrographs on scour around pier in sharp bend under incipient motion and live bed conditions. *International Journal of Civil Engineering*, *19*(1):51-65. https://doi.org/10.1007/s40999-020-00558-9
[27]. Mulahasan S, Al-Osmy S, Alhashimi S (2021, March) Modelling of flow pattern in an open channel with sidewall obstruction. In IOP Conference Series: Materials Science and Engineering, 1090(1):012097. IOP Publishing. doi:10.1088/1757-899X/1090/1/012097
[28]. Vaghefi M, Moradi S, Abdi Chooplou Ch (2021) Numerical Study of Bed Topography Variations Owing to Placement of Triad Series of Vertical Bridge Piers Installed in a 180-degree Bend with Different Relative Radii Using SSIIM Numerical Model. Iranian Journal of Science and Technology, Transactions of Civil Engineering, 45(3):1971-1988. https://doi.org/10.1007/s40996-020-00559-7
[29]. Indulekha K.P, Jayasree P.K, Sachin S (2021, March) Simulation of flow pattern around series of groynes with different orientations in meandering channels. In IOP Conference Series: Materials Science and Engineering 1114(1): 012024. IOP Publishing. doi:10.1088/1757-899X/1114/1/012024
[30]. Das L, Khatua K.K, Das B.S (2022) Experimental and Numerical Analyses of Boundary Shear Stress in Non-prismatic Compound Channel. In River Hydraulics (pp. 37-58). Springer, Cham https://doi.org/10.1007/978-3-030-81768-8_4
[31]. Chakravarthy V, Prasanna S.V.S.N.D.L, Suresh Kumar N (2022) Estimation and Simulation of Flows into an off-Taking Canal Using ANSYS. In Advanced Modelling and Innovations in Water Resources Engineering (pp. 21-29). Springer, Singapore. https://doi.org/10.1007/978-981-16-4629-4_2
[32]. Tripathi R.P, Pandey K.K (2022) Numerical investigation of flow field around T-shaped spur dyke in a reverse-meandering channel. Water Supply, 22(1):574-588. https://doi.org/10.2166/ws.2021.253
[33]. Rodi W (1993) Turbulence models and their application in hydraulics. CRC Press.
[34]. Vaghefi M, Faraji B, Akbari M, Eghbalzadeh A (2018) Numerical investigation of flow pattern around a T-shaped spur dike in the vicinity of attractive and repelling protective structures. Journal of the Brazilian Society of Mechanical Sciences and Engineering, 40(2):1-15. DOI: 10.1007/s40430-017-0954-y
[35]. White F.M (2011) Fluid mechanics. Mcgraw-Hill series in mechanical engineering, 7th edition.
[36]. Shukry A (1950) Flow around Bends in an open Flume. Transactions of the American Society of Civil Engineers, 115(1):751-779.